scientific reports

Check for updates

OPEN

An *in vitro* study for reducing the cytotoxicity and dose dumping risk of remdesivir via entrapment in nanostructured lipid carriers

Fatemeh Amiri, Sepideh Ziaei Chamgordani & Hedayatollah Ghourchian

The aim of this study was to synthesize and evaluate nanostructured lipid carriers (NLCs) loaded with Remdesivir (RDV) to control its side effects in COVID-19 patients. Due to the low solubility and short half-life of RDV in the blood, an injectable formulation was prepared using sulphobutylether-beta-cyclodextrin. However, it can accumulate in the kidney and cause renal impairment. NLCs improve the parenteral delivery of hydrophobic drugs such as RDV by increasing drug solubility and bioavailability. For the synthesis of RDV-NLCs, the aqueous phase containing Tween 80 was injected into the lipid phase under rapid stirring and was sonicated. The experimental conditions were optimized using Box-Behnken design and Design Expert software. The optimum formulation contained a total lipid of 2.13%, a total surfactant of 1%, and a hot bath time of 71 min. The optimum formulation showed particle size, polydispersity index, zeta potential, and entrapment efficiency values of 151.0 ± 1.7 nm (from 149.1 to 152.1), 0.4 ± 0.1 (from 0.3 to 0.5), −43.8 ± 1.2 mV (from −42.4 to −44.7), and 81.34 ± 1.57% (from 79.52 to 82.33%), respectively. RDV-NLCs showed acceptable stability for 30 days at 25 ℃ and were compatible with commonly used intravenous infusion fluids for 48 h. FE-SEM images of RDV-NLC showed spherical particles with a mean diameter of 207 nm. The NLC-RDV formulation showed a sustained release of RDV with a low risk of dose-dumping, minimizing potential side effects. In addition, RDV in the form of RDV-NLC causes less cytotoxicity to healthy normal kidney cells, which is expected to reduce renal impairment in COVID-19 patients.

At the beginning of 2020, the world faced a new coronavirus disease named COVID-19 by the World Health Organization (WHO). This infection is caused by the severe acute respiratory syndrome coronavirus 2 (SARS-CoV-2)[1]. To date, WHO has reported about 768 million confirmed cases of COVID-19, resulting in nearly 7 million deaths globally. The outbreak is defined as a pandemic, but no specific drug is available for its treatment. SARS-CoV-2 belongs to beta-coronaviruses, which also include SARS-CoV and MERS-CoV. The novel coronavirus has an 80% homology with the coronavirus associated with the acute respiratory syndrome (SARS-CoV), which became widespread in China in 2002, and some of its enzymes have more than 90% homology. A "conventional drug in new use" becomes a feasible solution when a newly synthesized drug is not immediately available for patients.

Remdesivir (RDV) has shown activity against SARS and MERS in animal and in vitro models, both of which belong to the coronavirus family, theoretically supporting its effectiveness in treating COVID-19[1]. Studies conducted by the Wuhan Institute of Virology on the effect of RDV on COVID-19 have shown that this drug is one of the fastest and most potent antiviral agents available for this disease[2].

RDV (GS-5734), a prodrug, is metabolized inside cells into an alanine metabolite (GS-704277), which is further processed into the monophosphate derivative and finally into the active nucleoside triphosphate derivative. The produced nucleoside triphosphates can then be mis-integrated into viral RNA by the viral RNA-dependent RNA polymerase for genome replication[3]. RDV, as an RNA-dependent RNA polymerase inhibitor, can inhibit the replication of multiple coronaviruses in respiratory epithelial cells. According to Gordon et al., the triphosphate form of RDV competes with its natural counterpart, ATP[4]. Once remdesivir is added to the growing chain, it cannot cause an immediate stop. On the contrary, it will continue to extend three more nucleotides down to stop the strand[1].

Laboratory of Bioanalysis, Institute of Biochemistry & Biophysics, University of Tehran, Enghelab Ave, P.O. Box: 13145-1384, Tehran 1417614411, Iran. ✉email: ghourchian@ut.ac.ir

As per the FDA protocol, the recommended dosage of RDV for COVID-19 treatment is a single loading dose of 200 mg on Day 1, followed by once-daily maintenance doses of 100 mg from Day 2 infused over 30 to 120 min via intravenous (IV) infusion. The recommended total treatment duration is 5 to 10 days. In patients with renal impairment, RDV is not recommended for those with an estimated glomerular filtration rate (eGFR) of less than 30 mL/min[5].

The most common side effects of RDV for COVID-19 include acute respiratory failure and organ dysfunction, hypoalbuminemia, hypokalemia, anemia, and thrombocytopenia[6]. The use of RDV for COVID-19 has been associated with potential kidney damage, such as renal and urinary disorders and renal tubular necrosis[7]. This is mainly because of renal clearance of RDV, with 74% excreted in the urine[8]. Additionally, the low solubility of RDV in water (0.339 mg/ml)[9] leads to its low bioavailability and requirement for multiple doses to achieve therapeutic drug levels[3]. To resolve this problem, sulfobutylether-beta-cyclodextrin has been reported to be used in an injectable formulation. The mentioned reagent also has renal clearance and may accumulate in the kidney of COVID-19 patients with renal impairment. Therefore, an efficient alternative formulation for better delivery of RDV with minimum side effects is required.

Nanosized drug-carrier systems have been developed in the past decades and are divided into polymeric and lipid nanoparticles[10]. Polymeric nanoparticles are solid colloidal particles made of non-biodegradable synthetic polymers or biodegradable macromolecular materials from synthetic, semisynthetic, or natural resources. They have some disadvantages, such as the cytotoxicity of polymers and the lack of suitable large-scale production techniques. In contrast, lipid nanoparticles have less toxicological risk due to the natural and biological origins of their materials. Solid lipid nanoparticles (SLNs) and nanostructured lipid carriers (NLCs) are the most common lipid nanomaterials. The advantages of SLNs are the use of biodegradable physiological lipids, the avoidance of organic solvents related to the production method, the possibility of large-scale production, improving the drug bioavailability, the protecting of sensitive drugs from rigorous environments, and controlling drug release[11]. Nevertheless, SLNs show disadvantages such as unpredictable gelation tendency, unexpected dynamics of polymorphic transitions, particle growing, high water content of SLN dispersions, adjustment of drug release profile, limited drug loading (DL) capacity due to the crystalline structure of solid lipids, and drug expulsion during storage due to the formation of a perfect crystal[12].

NLCs are the second generation of SLNs, which were developed to resolve some problems raised by SLNs. In contrast to SLN being produced from solid lipids, NLCs are produced by controlled mixing of solid lipids with liquid lipids, leading to unique nanostructures in the matrix. Since liquid lipids solubilize lipophilic molecules more than solid lipids, the NLC particles can provide a higher loading capacity and better release control. When SLNs are prepared from solid lipids, their matrix forms a perfect crystal lattice with limited space to accommodate the active ingredients. In contrast, the employment of solid and liquid lipids in NLCs can distort the production of a perfect crystal. The NLC matrix contains imperfections, providing space to accommodate the drug molecules in amorphous clusters, which can avoid drug expulsion. In the SLN, the drug is mainly dispersed in molecular form, while NLCs are composed of oily droplets embedded in a solid lipid matrix. Moreover, NLCs offer several other advantages, including better stability, a simple manufacturing process, biocompatibility, controlled drug release, improved performance in producing final dosage forms such as creams, tablets, capsules, injectables, and production of suspensions with higher solid content (e.g., 30–50% solid)[12,13].

Altogether, it seems that the incorporation of RDV into NLCs offers many advantages, such as improving the solubility of the drug, enhancing bioavailability, and increasing the half-life of the drug after intravenous injection. In addition, it is expected that NLCs provide a controlled and sustained RDV release to minimize the required doses for achieving therapeutic drug levels and preventing RDV side effects on body organs.

Response surface methodology is a cluster of mathematical and statistical techniques that helps analyze and model formulation obstacles. The most important purpose of this technique is to optimize the response surface, which is influenced by various process parameters. In addition, response surface methodology computes the relationship between the obtained response surfaces and the controllable input parameters[14]. As a response surface methodology, the Box-Behnken experimental design (BBD) is an excellent statistical method for optimizing formulations with multiple variables. Identifying the most significant factors for a response variable can minimize the trials required to determine the optimal formulation[15]. Thus, BBD can reduce the cost of the experiments and the researchers' time by reducing the complex experimental parameters and simplifying the experiments.

This study utilized BBD to optimize the NLCs for RDV and investigate the impact of various variables on particle size, polydispersity index, zeta potential, and entrapment efficiency (EE). Then, the physicochemical characteristics of the NLCs, including their in vitro drug release properties and compatibility with infusion fluids, were evaluated. This vital information can aid in the practical application of the formulation, particularly for drug delivery. Finally, assessing the relative cytotoxicity of RDV–NLC to RDV suspension in the Vero cell provided valuable insights into the formulation's potential safety and efficacy compared to the conventional drug formulations.

Materials and methods

Materials

RDV (≥ 99%) was obtained as a gift sample from Sobhan Oncology, Tehran, Iran. Medium-chain triglyceride (MCT; Nutricia Co., Ireland) was used as liquid-lipid, and glycerol monostearate (GMS; Sigma-Aldich) and stearic acid (SA; Merck Co., Germany) were used as solid-lipid materials of NLC. Lecithin from soybean was purchased from Serva Co. (Germany), and Tween 80 was purchased from Sigma. All other chemicals used in the study were of analytical grade. Additionally, all formulations were prepared using double-distilled deionized water. For cell culture studies, Dulbecco's modified eagle medium (DMEM) and fetal bovine serum (FBS) were purchased from Gibco (Grand Island, NY, USA). 0.25% trypsin–EDTA was purchased from DACell Co. (Tehran,

Iran). Dimethyl sulfoxide (DMSO; Merck Co., Germany), streptomycin/penicillin (PAN-Biotech Co, Aidenbach, Germany), and [3-(4,5- dimethylthiazol-2-yl)-2,5-diphenyltetrazolium bromide] (MTT) were purchased from Sigma and stored at -4 °C in the dark. The Vero cell line (derived from the kidney of an African green monkey, ATCC: CCL-81) was obtained from the Pasteur Institute of Iran (Tehran, Iran).

Methods

Preparation of RDV-NLC

RDV-NLC was prepared by the emulsion evaporation at a high temperature and solidification at a low temperature. The synthesis was performed under atmospheric pressure, and the lipid and aqueous phases were prepared separately. Briefly, total lipids (GMS:SA:MCT with the weight ratio of 3:2:1, respectively)[16], RDV, and lecithin were mixed and wholly dissolved in ethanol at 75 ± 2 ℃ (temperature above the melting point of the solid lipids) in a water bath to get the lipid phase. Wang et al. have previously reported that the mentioned NLCs lipid composition showed a high negative zeta potential value[16], mainly due to the carboxyl groups in MCT structure[17], indicating an excellent long-term stability of the formulation. Furthermore, a biphasic drug release pattern was found with drug burst release at the initial stage, followed by a sustained release at a constant rate. The negative charges may also protect against agglomeration of the prepared nanoparticles by generating adequate repulsive forces[18]. MCT can also help encapsulate a higher amount of drugs and reduce particle crystallinity, which imparts better stability and higher suitability for controlled release[16].

Tween 80 was dissolved entirely into the water and heated to the same temperature as the lipid phase to obtain a clear aqueous phase. The Tween 80/lecithin ratio of 8:1.2 was kept constant in all formulations, where it was previously reported to show good chemical and physical stability[19,20]. The aqueous phase (Tween 80/lecithin) was injected into the lipid phase within the isothermal condition under rapid stirring at 1200 rpm for 71 min to get the homogeneous emulsion[14]. The resulting hot lipid emulsion was probe sonicated for 20 min[15]. In order to acquire RDV-NLC dispersions, the obtained hot nanoemulsion was quickly dispersed into cold deionized water (0–2 ℃) under stirring at 1200 rpm for 2 h. The blank NLCs (without RDV) were also prepared using the same procedure[21]. Phosphatidylinositol and other anionic components in the lecithin contribute to the negative charge and stability of the emulsion. In particular, the mentioned ratio (8:1.2) caused a more negative zeta potential than the critical value of −30 mV for NLC particles[14]. All steps must be done consecutively and without interruption to ensure the stability of the emulsion during the preparation process. The optimized formulation was stored in a glass vial covered with aluminum foil in a refrigerator at 4 ℃ for further investigations[14]. Also, for FE-SEM microscopy, the sample was prepared in the form of powder using the freeze-drying method.

The hot emulsification followed by the probe sonication technique used for RDV-NLC preparation in this study showed simplicity and easy scaling up for industrial applications[22]. Although the increase in the batch size can lead to changes in formulation characteristics like EE, size, and PDI of the NLCs, Rapalli et al. showed reduced entrapment and enhanced size during the scale-up of nanoparticles[22].

BBD for optimization of NLC parameters

BBD helps evaluate critical experimental conditions with the maximum and minimum response, eliminating non-specific factors that do not affect the response variable and providing an optimized formulation with fewer trials. Based on a review of previous studies, specific parameters that could directly influence the desirable and optimum properties (particle size, polydispersity index, zeta potential, and EE) of the NLC system for intravenous delivery are total lipid content, total surfactant content, and hot bath time[14,15]. Furthermore, constraints were set on each factor influencing the formulation characteristics. A three-factor and three-level BBD was employed to optimize NLC using design expert 13.0.5.0 software (Stat-Ease Inc., Minneapolis, MN). BBD of three factors, namely, total lipid content (X_1), total surfactant content (X_2), and hot bath time (X_3) at three different levels (low, medium, and high) were employed to investigate their effects on responses, including particle size (Y_1), polydispersity index (Y_2), zeta potential (Y_3) and EE(Y_4).

Characterization of RDV–NLC

The parameters such as particle size, zeta potential, and polydispersity index of the prepared RDV–NLC were determined by dynamic light scattering (DLS) and zeta potential analyzer (SZ-100z, Horiba Jobin Jyovin, Japan) at 25 ℃. All the dispersion samples were diluted with deionized water to obtain a suitable concentration for measurement. Each sample was determined in triplicate[16,21].

The morphology of prepared RDV-NLC was determined using field emission scanning electron microscopy (FE-SEM, MIRA3, TESCAN, Czech Republic). The sample was prepared in the form of powder using the freeze-drying method. After coating with gold, electron microscope images of the sample were prepared with different magnifications[15].

Entrapment efficiency and drug loading

The EE and DL of RDV-NLC were determined by the centrifugal ultrafiltration method[21]. To determine the amount of free RDV from encapsulated one, 0.5 mL of RDV-NLC colloidal solution was diluted with 3.5 ml of ethanol 50% to avoid deposition (possibly via crystallization) of free RDV onto the NLC surface[23]. Then, the sample was placed in the upper chamber of a centrifuge tube matched with an ultrafilter (Amicon Ultra-15, Millipore Co., USA, MWCO 10 kDa) and centrifuged at 4000 rpm (CF16RX II, Hitachi, Japan) at 25 ℃ for 15 min[24,25]. Thus, the encapsulated drug (RDV-NLC) remained in the upper chamber, and the aqueous phase (containing free RDV) moved into the sample recovery chamber through a filter membrane[26]. The rinsed optimized formulation was used for the in vitro release experiment[27]. The filtrate was collected, diluted with ethanol 50%, and measured at 245 nm using a nano-drop UV spectrophotometer (2000C, Thermo, USA)[28]. Thereafter, using the

data of UV absorption of solutions in the concentration ranges from 16.5 to 200 µg/ml, a calibration curve with the regression equation of $y = 0.0062x + 0.0508$ and $R^2 = 0.99$ was plotted[29,30]. Then, using the UV absorption of the solution in the lower chamber and the regression equation of the related calibration curve, the amount of free RDV was calculated. *EE*% and *DL*% were calculated using Eqs. (1) and (2):

$$EE\% = 100 \times [(W_{total} - W_{free})/W_{total}]. \quad (1)$$

$$DL\% = 100 \times [(W_{total} - W_{free})/W_{NLC}], \quad (2)$$

where W_{Total}, W_{Free}, and W_{NLC} represent the weight of total RDV, free RDV, and NLC particles, respectively[30].

X-Ray diffraction (XRD) analysis of RDV-NLC

XRD patterns of both RDV and RDV-NLC (freeze-dried) were obtained using an X-ray diffractometer (Rigaku, Ultima IV, Japan) for equivalent amounts of samples. The range of 2θ angle scanning was 5–50° with a voltage of 40 kV and a current of 40 mA[31].

Physical stability of RDV-NLC

The storage stability of RDV-NLCs was studied by storing the optimized formulation in a glass vial covered with aluminum foil at 4 and 25 ℃. To prevent bacterial growth, 0.02% (w/v) sodium azide was added to the RDV-NLC suspension[32]. Samples were withdrawn after 30 days of storage and assessed for changes in physical appearance, particle size, polydispersity index, zeta potential, and EE[33,34].

In vitro release assay

A conventional dialysis diffusion method was chosen to investigate RDV release[21]. The dialysis membrane physically separates free RDV from RDV-NLC since only the released drug can pass through the membrane[35]. Immediately after the separation of free RDV from optimized NLC formulations, the drug release study was performed using a dialysis cellulose membrane. Three mL of RDV-NLC (containing three mg RDV) was put into a dialysis bag (MW cutoff 3.5 kDa, Sigma–Aldrich, USA) and sealed from both ends.

The dialysis bag was placed in 200 mL dissolution medium (PBS/ethanol, 1:1, v/v, pH 7.4)[36] and stirred with a magnetic stirrer under 100 rpm at 37 ± 0.5 ℃ for 72 h[16]. Aliquots of 2 mL were withdrawn at selected time intervals and were replaced with a fresh dissolution medium to maintain a constant volume (200 mL)[21]. The samples were analyzed by UV–Vis spectroscopy at 245 nm. To control the release of RDV from the RDV solution, 3 mg of RDV was dissolved in 3 ml of PBS/ethanol (1:1, v/v) and put into the dialysis bag. Then, the experiment was followed the same way as that mentioned for RDV-NLC. RDV calibration curve was plotted using RDV solutions in PBS/ethanol (1:1, v/v) by the UV–Vis spectroscopy method. The in vitro dissolution of RDV from RDV solution and RDV-NLC was statistically analyzed[15].

Evaluation of compatibility with infusion fluids

The compatibility assessment with different injectable diluents was studied to ensure the safety of parenteral infusion delivery. RDV-NLC was diluted with two commonly used intravenous infusion fluids, including 0.9% sodium chloride solution (normal saline) and distilled water (sterile water for injection). After dilution, the formulation compatibility was assessed, and the formulations were observed for any signs of precipitation or phase separation. The diluted solution particle size, polydispersity index, and EE were determined after 48 h at 25 ℃[37–39].

In vitro cytotoxicity study

The Vero cell line was initiated in 1962 from the kidney tissue derived from a normal, adult African green monkey (*Cercopithecus aethiops*)[40]. The Vero cell line has been widely used in virus replication studies and plaque assays[41,42]. The cytotoxic effects of RDV, blank NLC, and RDV-NLC on Vero cells were evaluated using cell cytotoxicity assay. Briefly, monolayers of Vero cells (1×10^4 cells/well) grown in 96-well plates were incubated with RDV solution, blank NLC, and RDV-NLC for 24, 48, and 72 h. The concentration of NLC in either blank NLC or RDV-NLC ranged from 0.03 to 2.81 mM in the culture medium[41]. Since RDV has low solubility in water, it cannot be diluted directly with the culture medium; thus, it was dissolved in DMSO 0.5%[41] and then diluted in the culture medium in the range of 0.5–44.22 µM.

After 24, 48, and 72 h, the cells were stained with MTT solution (50 mg/ml) and incubated for 4 h at 37 ℃. In the next step, the formed formazan crystals were dissolved in 100 µL DMSO, and the absorbance was determined at 570 nm using a microplate ELISA reader (Power wave XS2, Bio Tek, USA)[43]. The percentage of cell viability was calculated using Eq. 3:

$$Cell\ viability\% = 100 \times [(OD_t - OD_b)/(OD_c - OD_b)], \quad (3)$$

where OD_c, OD_b, and OD_t are the optical density of 'control' (non-treated Vero cells), culture medium, and treated Vero cells, respectively[44].

Statistical analysis

The statistical significance was calculated using the student's t-test, and the p-value of < 0.05 was considered significant. The results were reported as mean ± standard deviation.

Results

BBD analysis

The selected levels of independent variables used for BBD to prepare RDV-NLC were 1, 5.5, and 10% for X_1; 1, 3, and 5% for X_2; and 1, 2.5, and 4 h for X_3. Moreover, the selected goals for dependent variables (responses) were minimizing the Y_1 and Y_2 and maximizing the Y_3 and Y_4. As shown in Table 1, the design was composed of 15 experimental runs. Table 1 shows the observed responses in BBD for optimization of RDV-NLC formulation.

Polynomial equations were created by Design-Expert Software, which signified the mathematical linkages between the factors and the observed responses and checked for their significance by ANOVA, considering two conditions; first, the model is considered adequately fitting when the lack of fit p-value is > 0.1, i.e., non-significant. Second, the effectiveness of each independent factor is considered significant when the effect does not equal zero, and its p-value is < 0.05. Generally, a positive sign is assigned for the positive factor effect, whereas a negative sign represents the negative effect.

The design suggested that the most appropriate models for analyzing Y_1, Y_2, Y_3, and Y_4 are quadratic, linear, two-factor interaction, and quadratic models, respectively. The model terms were significant for all responses, whereas the lack of fits was non-significant, thus proving the adequacy of model fits.

The estimated effects of the independent variables on dependent factors, their level of significance, and associated p-values for the responses are presented in Tables 1 and 2. As shown, the model terms are significant for all responses, whereas the lack of fits are non-significant, thus proving the adequacy of model fits.

Effects on particle size

The design suggests that the quadratic model is the most appropriate model for analyzing the response (Y_1). As shown in Table 2, the model terms are significant ($p = 0.0098$), whereas the lack of fit is non-significant ($p = 0.8739$), thus proving the adequacy of model fit. The influence of different factors and their interactions on particle size in terms of actual factors could be represented by Eq. (4):

$$Particle\ size(Y_1) = -10.816 + 48.564X_1 - 7.143X_1X_3 + 11.855X_2X_3 - 2.012X_1^2 - 4.517X_2^2. \quad (4)$$

Total lipid content (X_1 at $p = 0.0116$) showed a significant positive effect on particle size. This positive effect can be attributed to a decrease in the emulsifying efficiency of surfactant and an increase in particle agglomeration[45]. Moreover, higher total lipid content increases the viscosity and the surface tension, resulting in higher particle size[33].

Effects on polydispersity index

The design suggests that the linear model is most appropriate for analyzing the response (Y_2). As shown in Table 2, the model terms are significant ($p = 0.0280$), whereas the lack of fit is non-significant ($p = 0.8171$), thus proving the adequacy of model fit. The X_2 parameter refers to the total surfactant content (Tween 80 and lecithin), which at $p = 0.0280$ showed a significant positive effect on the polydispersity index. This finding is consistent with previous reports[46].

The influence of total surfactant content (X_2) on the polydispersity index in terms of actual factors could be represented by Eq. (5):

Formulation code	Independent variables			Dependent variables			
	Total lipid (%)	Surfactant (%)	Hot bath time (h)	Y_1: Particle size (nm)	Y_2: Polydispersity index	Y_3: Zeta potential (mV)	Y_4: *EE* (%)
F1	5.5	5	1	84.13 ± 46.28	0.34 ± 0.01	−40.88 ± 0.63	75.47 ± 0.08
F2	5.5	1	1	191.33 ± 19.66	0.43 ± 0.01	−42.15 ± 1.89	79.1 ± 2.68
F3	5.5	3	2.5	197.07 ± 61.06	0.35 ± 0.01	−45.82 ± 0.52	83.65 ± 0.07
F4	1	3	1	58.97 ± 11.31	0.24 ± 0.01	−44.46 ± 3.89	81.92 ± 0.04
F5	1	3	4	111.47 ± 16.50	0.23 ± 0.01	−30.99 ± 4.81	70.38 ± 0.04
F6	10	3	4	130.07 ± 11.90	0.96 ± 0.00	−46.4 ± 9.63	87.04 ± 0.13
F7	10	3	1	189.87 ± 5.28	0.41 ± 0.00	−49.56 ± 3.35	81.7 ± 0.03
F8	5.5	3	2.5	176.17 ± 40.17	0.36 ± 0.01	−46.3 ± 3.67	84.89 ± 0.15
F9	5.5	1	4	65.61 ± 0.60	0.29 ± 0.00	−42.6 ± 1.41	75.98 ± 5.56
F10	5.5	5	4	128.7 ± 10.30	1.00 ± 0.00	−57.90 ± 9.50	88.04 ± 0.07
F11	5.5	3	2.5	105.83 ± 2.32	1.00 ± 0.00	−37.60 ± 9.32	100 ± 00
F12	1	1	2.5	4.57 ± 0.05	0.18 ± 0.00	−45.2 ± 7.95	86.82 ± 0.05
F13	10	1	2.5	80.23 ± 2.17	0.45 ± 0.01	−43.22 ± 2.05	82.74 ± 0.09
F14	1	5	2.5	38.80 ± 12.75	1.00 ± 0.00	−47.8 ± 9.03	82.06 ± 0.45
F15	10	5	2.5	158.70 ± 10.76	1.00 ± 0.00	−55.1 ± 9.77	89.53 ± 0.05

Table 1. Observed responses in BBD design for optimization of RDV-NLC formulation. The particle size, polydispersity index, and zeta potential were measured by the DLS technique. *EE*% was calculated using Eq. (1). *BBD* box-behnken experimental design, *NLC* nanostructured lipid carrier, *RDV* remdesivir.

Response	Particle size		Polydispersity index		Zeta potential		Entrapment efficiency	
	Factor effect	*p*-value	Factor effect	*p*-value	Factor effect	*p*-value	Factor effect	*p*-value
	Model (Quadratic)	0.0098	Model (Linear)	0.0280	Model (Two-factor interaction)	0.0385	Model (Quadratic)	0.0163
	Lack of fit	0.8739	Lack of fit	0.8171	Lack of fit	0.7392	Lack of fit	0.3490
Factor	**Coefficient estimate**	***p*-value**	**Coefficient estimate**	***p*-value**	**Coefficient estimate**	***p*-value**	**Coefficient estimate**	***p*-value**
Intercept	160.89		0.5489		−46.23		84.27	
X_1	38.58	0.0116	–	–	–	–	0.6850	0.3552
X_2	–	–	0.2491	0.0280	−3.56	0.0336	1.31	0.0840
X_3	–	–	–	–	−2.30	0.1704	2.20	0.0394
$X_1 X_2$	–	–	–	–	–	–	2.89	0.0283
$X_1 X_3$	−31.02	0.1063	–	–	–	–	7.81	0.0047
$X_2 X_3$	42.74	0.0354	–	–	−4.14	0.0705	3.92	0.0124
X_1^2	−42.67	0.0413	–	–	–	–	−0.9787	0.3510
X_2^2	−45.06	0.0332	–	–	–	–	2.00	0.1102
X_3^2	–	–	–	–	–	–	−6.62	0.0050

Table 2. Estimated effects of factors and associated *p*-values for the responses.

$$Polydispersity\ index(Y_2) = 0.175 + 0.125X_2. \tag{5}$$

Effects on zeta potential

The design suggests that the most suitable model for analyzing the response (Y_3) is the two-factor interaction model. As shown in Table 2, the model terms are significant ($p = 0.0385$), whereas the lack of fit is non-significant ($p = 0.7392$), thus proving the adequacy of model fit. Generally, higher |zeta potential| is preferable for optimizing nanoparticles and nanovesicles, and increasing zeta potential increases their physical stability. The data revealed that total surfactant content (X_2 at $p = 0.0336$) showed a significant negative effect on zeta potential values, and higher total surfactant content increased |zeta potential|. The increased negative charge of nanoparticles is due to the negative charge of surfactant molecules. Hot bath time (X_3 at $p = 0.1704$) did not show a significant effect on zeta potential values.

The influence of different factors and their combination on zeta potential, in terms of actual factors, is represented by the Eq. (6):

$$ZP(Y_3) = -47.416 + 1.67X_2 + 2.611X_3 - 1.381X_2X_3. \tag{6}$$

Effects on entrapment efficiency

The BBD suggests that the quadratic model is the most suitable model for analyzing the response (Y_4). As shown in Table 2, the model terms are significant ($p = 0.0163$), whereas the lack of fit is non-significant ($p = 0.3490$), thus proving the adequacy of model fit. The data revealed that hot bath time (X_3) exhibited a significant positive effect ($p = 0.0394$) on *EE%* values. As shown, total lipid content (X_1 at $p = 0.3552$) and total surfactant content (X_2 at $p = 0.0840$) did not show any significant effect on *EE%* values. The influence of different factors and their interactions on the *EE%* of NLCs (Y_4), in terms of actual factors, could be presented by Eq. (7):

$$\begin{aligned} EE(Y_4) = {} & +93.453 - 3.17X_1 - 7.374X_2 + 5.891X_3 + 0.321X_1X_2 + 1.157X_1X_3 \\ & + 1.308X_2X_3 - 0.048X_1^2 + 0.499X_2^2 - 2.942X_3^2. \end{aligned} \tag{7}$$

Design-Expert software created an optimized formulation with an overall desirability of 0.773. Independent variables of the optimum formulation had the following values: total lipid content (X_1): 2.128%, total surfactant content (X_2): 1%, and hot bath time (X_3): 71 min. So, the optimized formulation was synthesized, and four responses were evaluated.

Particle size and zeta potential analysis

The analysis of particle size, polydispersity index, and zeta potential are essential for the evaluation of drug systems[21]. In the optimized conditions the RDV-NLC mean diameter was obtained by DLS technique as 151.0 ± 1.7 nm (from 149.1 nm to 152.1 nm) with a polydispersity index value of 0.4 ± 0.1 (from 0.3 to 0.5). This indicated a relatively narrow and uniform particle size distribution. Furthermore, the obtained mean zeta potential of −43.8 ± 1.2 mV (from −42.4 mV to −44.7 mV) indicated a negative charge at the surface of the nanoparticles. Phosphatidylinositol and other anionic components in lecithin contribute to the negative charge of NLCs[19,47]. Furthermore, hydroxyl groups of Tween 80 can also produce a slight negative charge.

Additionally, MCT produces a more negative charge due to its carboxyl groups. It should be noted that nanoparticle stabilization can also occur by a combination of electrostatic and steric forces caused by lecithin and Tween 80, respectively[17]. The presence of probable similar charges might protect against agglomeration of the prepared nanoparticle formulations by generating adequate repulsive forces[18]. As mentioned earlier, increasing

the zeta potential increases the physical stability of nanoparticles, and a minimum zeta potential of greater than −30 mV is required for good physical stability[48].

Entrapment efficiency and drug loading determination

The *EE*% and *DL*% are important appraisal factors for the preparation of lipid nanoparticles as drug carriers[21]. The centrifugation ultrafiltration method was chosen to evaluate these parameters because of its convenience and high efficiency compared to other methods[16]. The *EE*% and *DL*% of the optimized RDV–NLC was 81.34 ± 1.57% (from 79.52 to 82.33%) (n = 3) and 1.91 ± 0.04% (n = 3), respectively. These results can be attributed to the unique matrix structure of NLCs[31], the high affinity of the lipophilic drug RDV to GMS, SA, and MCT[31], and the low solubility of RDV in water (0.339 mg/ml)[9,49].

We also evaluated and compared the XRD patterns of RDV and RDV-NLCs to investigate the changes in RDV crystallinity after loading into NLC particles. As shown in Fig. 1, the characteristic peaks of RDV were not observed in RDV-NLCs, indicating that RDV was stabilized in an amorphous form in NLCs. This also confirms the successful entrapment of RDV in the lipid cores of NLCs[50]. XRD results were well-matched with previous reports in the literature[50,51].

In NLCs, the solid lipid matrix encloses tiny oil sections, leading to massive crystal order disturbance, which greatly affects drug EE to a great extent[31]. Therefore, incorporating the liquid lipid MCT in the solid lipids leads to a massive crystal order defect, resulting in a lipid matrix with imperfections in the crystal lattice[52]. These imperfections in the crystal matrix provide sufficient space to accommodate many drug molecules, subsequently leading to a high EE and DL capacity[31].

Morphology investigation

The FE-SEM images of RDV-NLC revealed spherical shapes with relatively smooth surfaces and particle diameters from 77 to 358 nm (207 nm on average) (Fig. 2). This size is well correlated with the particle size obtained from DLS (151 ± 1.7 nm). Furthermore, the occasional clumps (Fig. 2a) might be associated with the shrinkage of nanoparticles during drying or the concentration of the dispersion medium[31].

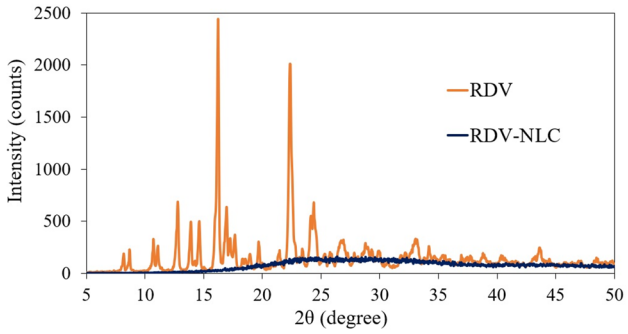

Figure 1. Comparison between XRD patterns of RDV and RDV-NLC.

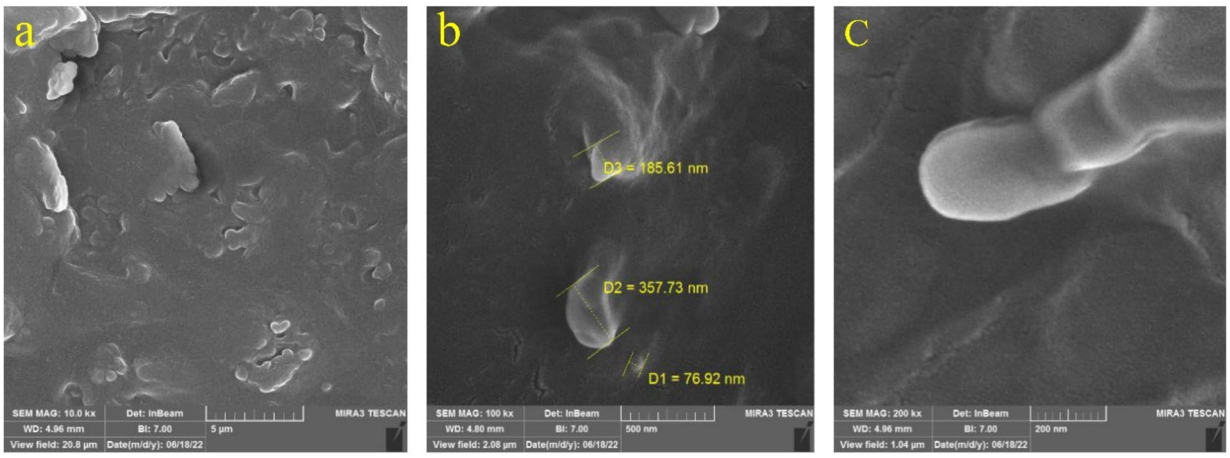

Figure 2. FE-SEM images of the optimized RDV-NLCs with three magnifications from (**a**) to (**c**): 10, 100, and 200 kx.

Physical stability of RDV-NLC

The physical stability studies of the RDV-NLCs were carried out through 30 days of storage at 4 ℃ and 25 ℃ independently and evaluated for changes in physical appearance, particle size, polydispersity index, zeta potential, and *EE*% (Table 3). RDV-NLCs showed no phase separation or noticeable change in appearance after a month compared to day one. However, the results indicated a decrease in the particle size and an increase in the polydispersity index. This could be attributed to the ongoing changes in lipid matrix crystallinity and polymorphic phase transitions[53]. In addition, the decrease in particle size may be due to drug expulsion, which is consistent with the increase in the polydispersity index and decrease in EE.

Moreover, there was no significant change in the zeta potential, indicating the stability of the developed formulation against lipid nanoparticle aggregation or agglomeration and gelation phenomena. This finding is in accordance with data reported in the literature[48]. Nevertheless, after 30 days, the *EE*% of RDV-NLCs decreased by about 23% and 17% at 4 ℃ and 25 ℃, respectively. This may be attributed to the polymorphic behavior of the solid lipids incorporated in the formulation of NLCs, which were presented as imperfect crystal and amorphous types in NLCs after the preparation. During storage, a few more perfect crystalline β-polymorphs of solid lipids in NLCs may be formed upon exposure to kinetic energy (light or temp), leading to slight drug expulsion[49,52–54].

An independent stability test has also been conducted to evaluate the *EE*% of RDV-NLC after 30 and 90 days. The results for stability of RDV-NLC after 3 months were satisfactory (Table 4).

Overall, the data indicated that RDV-NLCs are stable at both storage conditions with a slight change in parameters. In addition, they suggest 25 ℃ relative to 4 ℃ is a better storage temperature for RDV-NLCs[33].

Kinetics of RDV release

To consider the risk of RDV–NLC dose dumping, the release pattern of RDV solution and RDV–NLC was compared. To maintain the sink condition, PBS/ethanol (1:1, v/v) was used as the dissolution medium to improve the solubility of RDV[55].

Figure 3 represents the kinetics of RDV release from RDV solution and RDV–NLC while entrapped in a dialysis bag and stirred in PBS/ethanol. As seen, RDV showed a biphasic release pattern. However, the rate of RDV release from RDV–NLC was lower than that from RDV solution, indicating the control of RDV release by NLCs.

As seen, in the case of RDV solution, at the first 10 h, 90% of RDV is released from the dialysis bag (Fig. 3, blue curve). Thereafter, due to the equilibration of RDV concentration on both sides of the dialysis bag, the RDV release is almost stopped. However, in the case of RDV-NLC, the RDV release rate is much slower, so, at the first 6 h, just about 30% of RDVs are released. In the next step, a gradual and sustained release of about 10% is observed for more than 66 h.

The mechanism behind this biphasic slow-release pattern of RDV from NLC could be explained according to the hydrophobic structure of RDV, which tends to stay in the lipid matrix of NLC. It was previously reported that the drug could be incorporated between fatty acid chains, among the lipid layers, or in any imperfections in the NLC structure[56]. GMS and SA in the NLC structure rapidly solidified during the cooling process to form a solid lipid core due to their high melting points. Simultaneously, the MCT was encapsulated in this solid lipid core or distributed around it randomly. As MCT has higher solubility in nanodrug formulation, large amounts of the drug are loaded in the outer lipid layer. In the burst release stage, the RDV loaded in the shell was released easily and rapidly. Meanwhile, in the sustained release stage, RDV loaded in the solid lipid core is released by matrix degradation and erosion, which results in a prolonged release[57]. Other factors contributing to the fast release are the large surface area, low viscosity, and high diffusion coefficient of nanoparticles, as well as the short diffusion coefficient of RDV and surfactant concentration[58].

Characteristics	Temperature (℃)	First day	30th day
Particle size (nm)	4	151.0 ± 1.7	110.2 ± 6.9
	25	151.0 ± 1.7	126.2 ± 7.2
Polydispersity index	4	0.4 ± 0.1	0.7 ± 0.0
	25	0.4 ± 0.1	0.5 ± 0.1
Zeta potential (mV)	4	−44.5 ± 0.3	−44.6 ± 0.6
	25	−44.5 ± 0.3	−46.6 ± 1.6

Table 3. Changes in RDV-NLCs characteristics, measured by the DLS, with respect to time after storage at 4 or 25 °C. Each point represents the mean value of three measurements.

Characteristics	Temperature (℃)	First day	30th day	90th day
Entrapment efficiency (%)	4	81.3 ± 1.6	74.78 ± 0.75	72.92 ± 0.11
	25	81.3 ± 1.6	75.93 ± 0.24	65.86 ± 17.91

Table 4. Changes in RDV-NLCs *EE*% with respect to the times after storage at 4 or 25 ℃. Each point represents the mean value of three measurements. (*EE*% was calculated using Eq. 1).

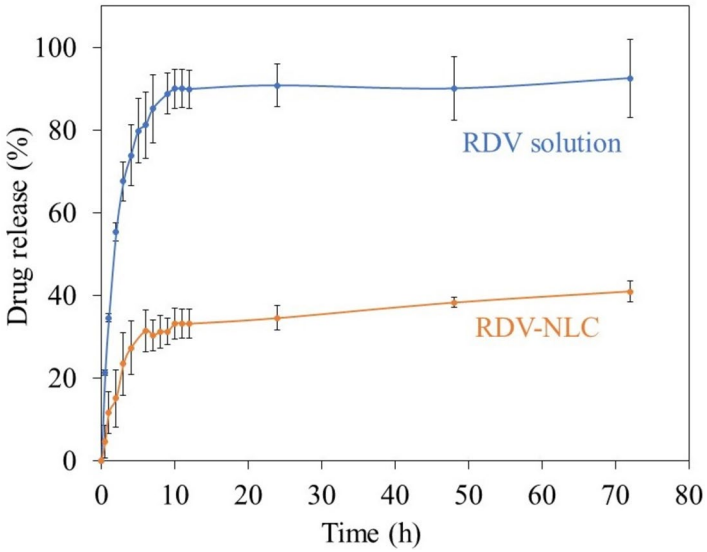

Figure 3. The in vitro release kinetics of RDV from RDV solution and RDV–NLC, entrapped in a dialysis bag and stirring in PBS/ethanol, 1: 1, v/v, pH 7.4, at 37 ± 0.5 °C for 72 h. Aliquots of 2 mL were withdrawn at selected time intervals and analyzed by UV–Vis at 245 nm. Each point represents the mean value of three measurements.

Thus, it seems that loading RDV into NLC particles leads to a controlled sustained-release pattern, which may decrease the risk of RDV dose dumping compared to RDV solution[15].

Compatibility with infusion fluids

Dilution of RDV-NLC in either saline or distilled water and then storing the samples up to 48 h at 25 ℃ revealed the compatibility of formulations with common injectable liquids so that no signs of phase separation or precipitation were observed. However, the diluted RDV-NLCs in normal saline showed a slight decrease in particle size (from 151 ± 1.7 nm to 135.6 ± 6 nm) and an increase in polydispersity index (from 0.4 ± 0.1 to 0.6 ± 0.1) after this period (Fig. 4). The decrease in particle size might be due to drug expulsion, which is in accordance with the increase in the polydispersity index and decrease in *EE*% (from 85 ± 2.6% to 78 ± 1.1%). In contrast, the diluted RDV-NLCs in distilled water showed a significant increase in particle size (from 151 ± 1.7 nm to 245 ± 12 nm) and polydispersity index (from 0.4 ± 0.1 to 0.7 ± 0.1), maybe due to the aggregation of nanoparticles in pure water. So, it seems that the lipid nanoparticles are more stable in 0.9% sodium chloride solution compared to pure water[39,59]. However, 0.9% sodium chloride prevents aggregation of lipid nanoparticles due to the creation of sodium cation (Na +) and chloride anion (Cl-).

Moreover, the *EE*% of RDV-NLCs diluted with normal saline decreased by 7% after 48 h, which might be attributed to the ongoing changes in lipid matrix crystallinity and polymorphic phase transitions[53]. In comparison, the *EE*% of RDV-NLCs in distilled water showed a 1.2% decrease (from 80.3 ± 0.1% to 79.1 ± 0.3%), which was not significantly different from before dilution. Therefore, the results indicated that the diluted RDV-NLCs, especially in the presence of saline, are generally compatible with commonly used infusion fluids over 48 h storage at room temperature[37–39].

In vitro cytotoxicity assay

The cytotoxicity effect of the blank NLC, RDV solution, and RDV-NLC on the Vero cell line was investigated for 24, 48, and 72 h (Fig. 5a–c). As shown in Fig. 5, NLC, either in the form of blank NLC or RDV-NLC, at low concentrations not only prevents cell cytotoxicity but also increases cell growth. It is probably because of the presence of MCT in the NLC structure, which can enhance cell growth and proliferation[60]. A specific receptor for MCT at the cell surface is GPCR84 (one of the G-protein coupled receptors family), which is expressed at the surface of the different cells of the body such as heart, lung, liver, bone marrow, kidney, immune cells, etc. After binding MCT to the receptor, the LYN protein is activated in its downstream signaling in the cytoplasm, which in turn activates the AKT pathway[61]. In the AKT pathway, BAD and FOXO proteins, which are involved in cell apoptosis, are deactivated, and instead, GSK and TSC proteins are activated, which play a role in cell growth and protein translation[62]. Additionally, soybean lecithin is a precursor for the production of fatty acids in the cell, and phosphatidylcholine is one of its derivations. Phosphatidylcholine metabolism plays a crucial role in cell survival and proliferative signaling by providing the major cellular membrane components[63].

However, the cell viability is decreased at higher concentrations of NLC. It has been proven that MCT can influence membrane characteristics and increase its fluidity. Thus, at higher concentrations, maybe through increasing the cell membrane permeability, MCT leads to more RDV uptake in the cell[64]. Enhancing the uptake of RDV can probably be an important issue for better treatment of COVID-19-infected cells with minimum side effects. Another reason for reducing cell viability in higher concentrations of NLC is probably the accumulation

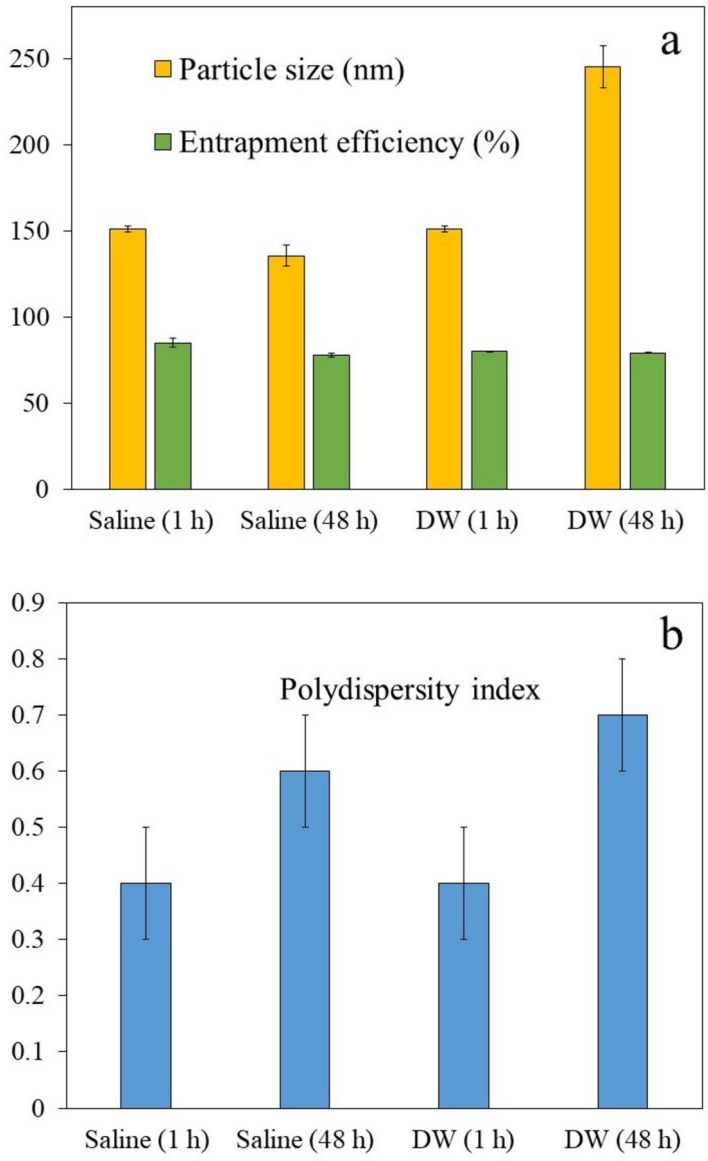

Figure 4. Particle size (a), *EE*% (**a**), and polydispersity index (**b**) of RDV-NLCs diluted either in saline or in distilled water (DW) after one and 48 h. Each point represents the mean value of three measurements.

of NLC particles at the surface of culture media, which prevents the oxygen supply to the cells and reduces their viability[65].

Furthermore, increasing the RDV concentration decreases the viability of the Vero cells, which is in accordance with previously reported studies[41]. Generally, due to the cytotoxicity of RDV, the RDV-NLC caused more cytotoxicity than the blank NLC at high concentrations. Figure 5a–c) indicated that cell viability decreases over time so that after 72 h, the toxicity of RDV and RDV-NLC were almost aligned at higher concentrations (> 25 µM of RDV and > 1.65 mM of NLC). The reason can be attributed to the sustained slow release of RDV from NLCs during 72 h of incubation, which was discussed in the previous section. On the other hand, the maximum cell densities cannot be greater than 50,000 cells/well in a 96-well plate[66]. According to the short doubling time of the Vero cell line (less than 24 h), decreasing the cell viability after 72 h may also be due to the saturation of wells and serum supply competition between cells.

However, RDV-NLC showed less cytotoxicity than RDV solution, especially in low to medium concentrations. Thus, it can be concluded that NLC reduces the cytotoxicity caused by RDV.

Recent clinical trials have shown that there is a significant relationship between acute kidney injury and RDV treatment in COVID-19 patients, especially for older patients or patients who suffer from kidney disorders[67]. Also, it has been proven that in RDV-treated COVID-19 patients, the rate of kidney glomerular filtration is reduced[68]. Therefore, the side effects of RDV cannot be ignored. However, the results of the MTT assay confirmed the negative effect of RDV and the positive effect of NLC components on cell viability. Additionally, the NLC component can make the cell membrane more permeable, so RDV-NLC likely has the potential to increase

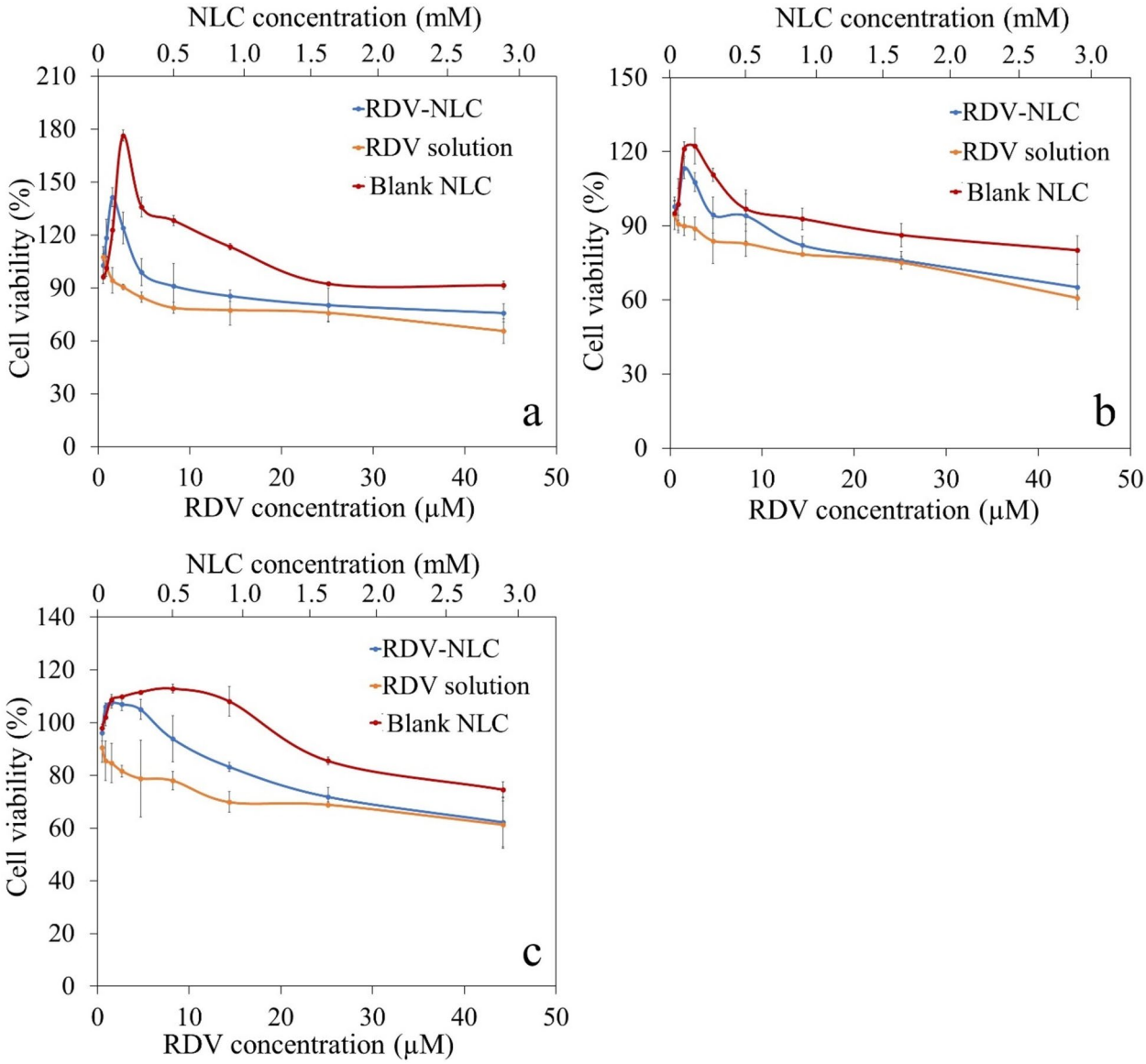

Figure 5. Cell viability of Vero cell line incubated with serial dilution of blank NLC, RDV solution, and RDV-NLC in culture media for 24 (**a**), 48 (**b**), and 72 h (**c**). The percentage of cell viability was calculated using Eq. (3). Each point represents the mean value of three measurements.

RDV uptake for better antiviral activity against COVID-19-infected cells. Thus, it seems that the proposed RDV-NLC formulation has the potential to be used as an alternative for RDV to reduce its side effects on body cells, especially kidney cells.

Comparison of RDV-NLC with previously reported RDV formulations

So far, the injectable formulation of RDV has been used for the treatment of COVID-19 patients, which was briefly criticized in the introduction section. To our knowledge, there is only one report on RDV-NLC formulation[50] with a different lipid composition (campul MCM and polyoxyethylene 40 stearate). In the mentioned report, the storage stability of RDV-NLC was not evaluated, and the obtained zeta potential (-6.84 ± 0.59 mV) was much lower than the advised critical value of |30| mV[14]. This probably leads to nanoparticles agglomeration and reduction of storage stability. In contrast, the present RDV-NLC formulation showed much higher negatively charged zeta potential (-43.8 ± 1.2 mV) with acceptable storage stability (30 days). It seems that in addition to the proper composition of NLCs, the optimization of the formulation by BBD, especially the evaluation of the impact of variables on responses, were important parameters that affected stability.

Moreover, we observed a more sustained release of RDV from NLC compared to that reported in[50], which might be due to the structure of lipids incorporated in NLC. In addition, as mentioned in the cytotoxicity assay section, our experimental results revealed that NLC (either in the form of blank NLC or RDV-NLC) not only showed less cytotoxicity against normal healthy cells but also increased cell growth. This evidence could explain

the role of NLC in reducing the RDV side effects on normal Vero cells, which has not been considered in the above-mentioned report.

It was previously reported that RDV-loaded Nanoliposomes stabilized by chitosan/hyaluronic acid film showed antiviral activity against the human coronavirus OC43[69]. Compared with nanoliposomes, the lipid core of NLCs provides better stability[70]. Since RDV has low solubility in water, the mixture of solid-oil lipid core of NLC could be maintained stable for a long-term storage period, which was evaluated in our study. However, the mentioned report did not evaluate the physical stability of RDV-nanoliposome. Moreover, compared to the thin-film hydration method utilized for nanoliposome production, the NLC synthesis procedure is simple, convenient, and cost-effective, which makes it optimum for large-scale production.

Discussion

The spherical RDV–NLC with an EE of 81.34 ± 1.57% (n = 3) and drug loading capacity of 1.91 ± 0.04% (n = 3) was synthesized. The relatively low negative zeta potential of −43.8 ± 1.2 mV in this formulation led to its acceptable stability. The in vitro RDV release assays revealed a biphasic controlled and sustained slow-release pattern that could prevent RDV dose-dumping compared to the RDV solution. Moreover, RDV-NLC formulation was compatible with the saline buffer as a commonly used intravenous infusion fluid. Additionally, in vitro cytotoxicity assay on Vero cells, as a kidney tissue cell line, implied that RDV–NLC caused less cytotoxicity than RDV solution, especially at low concentrations. In fact, at low concentrations, NLC not only prevents cytotoxicity against normal cells but also increases cell viability, probably due to the presence of MCT and soybean lecithin in its structure. On the other hand, enhancing the uptake of RDV due to increasing the membrane permeability is expected to be one of the influences of MCT in NLC structure. It is an important issue for better treatment of COVID-19-infected cells with minimum side effects, although further assays are required to confirm this point. Based on MTT results and according to the recent findings about the effect of RDV treatment on acute kidney injury, it is anticipated that RDV-NLC formulation has the potential to be an alternative intravenous slow-released drug delivery system for RDV with fewer side effects, including less cytotoxicity and the minimum risk of dose-dumping.

Even though the synthesis of the proposed formulation follows a simple method and it is easily possible to scale it up for mass consumption in the clinic, there are also possible challenges. First, as mentioned previously, compounds such as MCT can increase membrane fluidity at high concentrations. Although this effect will lead to an increase in RDV uptake into the cells, in higher concentrations, it can be cytotoxic because of membrane dilution. Second, there is also a stability challenge about lipid carriers. Relatively low stability of lipid carriers can limit the storage time of nano-drugs, especially in scaling up for broad clinical use. Therefore, for the commercialization of RDV-NLC formulation, the optimal concentration of the nano-drug and its storage time should be accurately considered. Furthermore, replacing the oral administration of RDV-NLC with intravenous administration needs an independent pharmacokinetic study that could be performed in the future.

Data availability

The authors confirm that the data supporting the findings of this study are available within the article. Also, the datasets generated during and/or analyzed during the current study are available from the corresponding author on reasonable request.

Received: 19 November 2023; Accepted: 12 August 2024
Published online: 21 August 2024

References

1. Cao, Y.-C., Deng, Q.-X. & Dai, S.-X. Remdesivir for severe acute respiratory syndrome coronavirus 2 causing COVID-19: An evaluation of the evidence. *Travel Med. Infect. Dis.* **35**, 101647. https://doi.org/10.1016/j.tmaid.2020.101647 (2020).
2. Wang, M. *et al.* Remdesivir and chloroquine effectively inhibit the recently emerged novel coronavirus (2019-nCoV) in vitro. *Cell Res.* **30**, 269–271. https://doi.org/10.1038/s41422-020-0282-0 (2020).
3. Eastman, R. T. *et al.* Remdesivir: a review of its discovery and development leading to emergency use authorization for treatment of COVID-19. *ACS Cent. Sci* **6**, 672–683. https://doi.org/10.1021/acscentsci.0c00489 (2020).
4. Gordon, C. J. *et al.* The antiviral compound remdesivir potently inhibits RNA-dependent RNA polymerase from Middle East respiratory syndrome coronavirus. *J. Biol. Chem.* **295**, 4773–4779. https://doi.org/10.1074/jbc.AC120.013056 (2020).
5. Adamsick, M. L. *et al.* Remdesivir in patients with acute or chronic kidney disease and COVID-19. *J. Am. Soc. Nephrol. JASN.* **31**, 1384 (2020).
6. Zadeh, N. M. *et al.* Mechanism and adverse effects of COVID-19 drugs: A basic review. *Int. J. Physiol. Pathophysiol Pharmacol.* **13**, 102. https://doi.org/10.1021/acscentsci.0c00489 (2021).
7. Silva, N.A.d.O., *et al.* Potential kidney damage associated with the use of remdesivir for COVID-19: Analysis of a pharmacovigilance database. *Cadernos de Saúde Pública* **37**, e00077721. https://doi.org/10.1590/0102-311X00077721 (2021).
8. Leegwater, E. *et al.* Population pharmacokinetics of remdesivir and GS-441524 in hospitalized COVID-19 patients. *Antimicrob. Agents Chemother.* **66**, e00254-e322. https://doi.org/10.1128/aac.00254-22 (2022).
9. Hanafin, P. O. *et al.* A mechanism-based pharmacokinetic model of remdesivir leveraging interspecies scaling to simulate COVID-19 treatment in humans. *CPT: Pharmacomet. & Syst. Pharmacol.* https://doi.org/10.1002/psp4.12584 (2021).
10. Sawant, K. K. & Dodiya, S. S. Recent advances and patents on solid lipid nanoparticles. *Recent Pat. Drug Deliv. Formul.* **2**, 120–135. https://doi.org/10.2174/187221108784534081 (2008).
11. Jores, K., Mehnert, W. & Mäder, K. Physicochemical investigations on solid lipid nanoparticles and on oil-loaded solid lipid nanoparticles: A nuclear magnetic resonance and electron spin resonance study. *Pharm. Res.* **20**, 1274–1283. https://doi.org/10.1023/A:1025065418309 (2003).
12. Shidhaye, S. *et al.* Solid lipid nanoparticles and nanostructured lipid carriers-innovative generations of solid lipid carriers. *Curr. Drug Deliv.* **5**, 324–331. https://doi.org/10.2174/156720108785915087 (2008).
13. Fang, C.-L., Al-Suwayeh, S. A. & Fang, J.-Y. Nanostructured lipid carriers (NLCs) for drug delivery and targeting. *Recent Pat. Nanotechnol.* **7**, 41–55. https://doi.org/10.1016/S0378-5173(02)00180-1 (2013).

14. Asfour, M. H., Kassem, A. A. & Salama, A. Topical nanostructured lipid carriers/inorganic sunscreen combination for alleviation of all-trans retinoic acid-induced photosensitivity: Box-Behnken design optimization, in vitro and in vivo evaluation. *Eur. J. Pharm Sci* **134**, 219–232. https://doi.org/10.1016/j.ejps.2019.04.019 (2019).
15. Jazuli, I. *et al.* Optimization of nanostructured lipid carriers of lurasidone hydrochloride using Box-Behnken design for brain targeting: In vitro and in vivo studies. *J. Pharm. Sci.* **108**, 3082–3090. https://doi.org/10.1016/j.xphs.2019.05.001 (2019).
16. Wang, Z. *et al.* Construction and in vitro/in vivo evaluation of 17-allylamino-17-demethoxygeldanamycin (17AAG)-loaded PEGylated nanostructured lipid carriers. *Drug Dev Ind. Pharm.* **42**, 91–98. https://doi.org/10.3109/03639045.2015.1031138 (2016).
17. Akhoond Zardini, A. *et al.* Production and characterization of nanostructured lipid carriers and solid lipid nanoparticles containing lycopene for food fortification. *J. food sci. Technol.* **55**, 287–298. https://doi.org/10.1007/s13197-017-2937-5 (2018).
18. Elsayed, I. & Sayed, S. Tailored nanostructured platforms for boosting transcorneal permeation: Box–Behnken statistical optimization, comprehensive in vitro, ex vivo and in vivo characterization. *Int. J. Nanomed.* **12**, 7947. https://doi.org/10.2147/IJN.S150366 (2017).
19. Charoenputtakhun, P. *et al.* All-trans retinoic acid-loaded lipid nanoparticles as a transdermal drug delivery carrier. *Pharm. Dev. Technol.* **19**, 164–172. https://doi.org/10.3109/10837450.2013.763261 (2014).
20. Chinsriwongkul, A. *et al.* Physicochemical properties of lipid emulsions formulated with high-load all-trans-retinoic acid. *PDA J. Pharm. Sci. Technol.* **61**, 461–471 (2007).
21. Wang, L. *et al.* PEGylated nanostructured lipid carriers (PEG–NLC) as a novel drug delivery system for biochanin A. *Drug Dev Ind. Pharm.* **41**, 1204–1212. https://doi.org/10.3109/03639045.2014.938082 (2015).
22. Rapalli, V. K. *et al.* Curcumin loaded nanostructured lipid carriers for enhanced skin retained topical delivery: Optimization, scale-up, in-vitro characterization and assessment of ex-vivo skin deposition. *Eur. J. Pharm. Sci.* **152**, 105438. https://doi.org/10.1016/j.ejps.2020.105438 (2020).
23. Karimi, N. *et al.* Antioxidant, antimicrobial and physicochemical properties of turmeric extract-loaded nanostructured lipid carrier (NLC). *Colloid Interface Sci. Commun.* **22**, 18–24. https://doi.org/10.1016/j.colcom.2017.11.006 (2018).
24. Bashiri, S. *et al.* Preparation and characterization of chitosan-coated nanostructured lipid carriers (CH-NLC) containing cinnamon essential oil for enriching milk and anti-oxidant activity. *LWT* **119**, 108836. https://doi.org/10.1016/j.lwt.2019.108836 (2020).
25. Luo, Q. *et al.* Nanostructured lipid carrier (NLC) coated with Chitosan Oligosaccharides and its potential use in ocular drug delivery system. *Int. J. Pharm.* **403**, 185–191. https://doi.org/10.1016/j.ijpharm.2010.10.013 (2011).
26. Gonzalez-Mira, E. *et al.* Optimizing flurbiprofen-loaded NLC by central composite factorial design for ocular delivery. *Nanotechnology* **22**, 045101. https://doi.org/10.1088/0957-4484/22/4/045101 (2010).
27. Aliasgharlou, L. *et al.* Nanostructured lipid carrier for topical application of N-acetyl glucosamine. *Adv. Pharm. Bull.* **6**, 581. https://doi.org/10.15171/apb.2016.072 (2016).
28. Mendes, A. *et al.* Miconazole-loaded nanostructured lipid carriers (NLC) for local delivery to the oral mucosa: Improving antifungal activity. *Colloids Surf. B: Biointerfaces* **111**, 755–763. https://doi.org/10.1016/j.colsurfb.2013.05.041 (2013).
29. Almousallam, M., Moia, C. & Zhu, H. Development of nanostructured lipid carrier for dacarbazine delivery. *Int. Nano Lett.* **5**, 241–248. https://doi.org/10.1007/s40089-015-0161-8 (2015).
30. Mahmoudi, S. *et al.* Targeted hyaluronic acid-based lipid nanoparticle for apigenin delivery to induce Nrf2-dependent apoptosis in lung cancer cells. *J. Drug Deliv. Sci. Technol.* **49**, 268–276. https://doi.org/10.1016/j.jddst.2018.11.013 (2019).
31. Gaba, B. *et al.* Nanostructured lipid carrier system for topical delivery of terbinafine hydrochloride. *Bull. Fac. Pharm. Cairo Univ.* **53**, 147–159 (2015).
32. Salminen, H. *et al.* Influence of encapsulated functional lipids on crystal structure and chemical stability in solid lipid nanoparticles: Towards bioactive-based design of delivery systems. *Food Chem.* **190**, 928–937. https://doi.org/10.1016/j.foodchem.2015.06.054 (2016).
33. Baruah, U. K. *et al.* Optimisation of chloroquine phosphate loaded nanostructured lipid carriers using Box-Behnken design and its antimalarial efficacy. *J. Drug Target.* **26**, 576–591. https://doi.org/10.1080/1061186X.2017.1390671 (2018).
34. Elmowafy, M. *et al.* Atorvastatin-loaded nanostructured lipid carriers (NLCs): Strategy to overcome oral delivery drawbacks. *Drug Deliv.* **24**, 932–941. https://doi.org/10.1080/10717544.2017.1337823 (2017).
35. Kim, Y. *et al.* Recent progress in drug release testing methods of biopolymeric particulate system. *Pharmaceutics* **13**, 1313. https://doi.org/10.3390/pharmaceutics13081313 (2021).
36. Behbahani, E. S. *et al.* Curcumin loaded nanostructured lipid carriers: In vitro digestion and release studies. *Polyhedron* **164**, 113–122. https://doi.org/10.1016/j.poly.2019.02.002 (2019).
37. Aboumanei, M. H. *et al.* Design and development of microemulsion systems of a new antineoplaston A10 analog for enhanced intravenous antitumor activity: In vitro characterization, molecular docking, 125I-radiolabeling and in vivo biodistribution studies. *Int. J. Pharm.* **545**, 240–253. https://doi.org/10.1016/j.ijpharm.2018.05.010 (2018).
38. Kharkar, P. B., Talkar, S. S. & Patravale, V. B. An industrially viable technique for fabrication of docetaxel NLCs for oncotherapy. *Int. J. Pharm.* **577**, 119082. https://doi.org/10.1016/j.ijpharm.2020.119082 (2020).
39. Prabhu, P. *et al.* Nanostructured lipid carriers of artemether–lumefantrine combination for intravenous therapy of cerebral malaria. *Int. J. Pharm.* **513**, 504–517. https://doi.org/10.1016/j.ijpharm.2016.09.008 (2016).
40. Osada, N. *et al.* The genome landscape of the african green monkey kidney-derived vero cell line. *DNA Res.* **21**, 673–683. https://doi.org/10.1093/dnares/dsu029 (2014).
41. Ma, Q. *et al.* Liu Shen capsule shows antiviral and anti-inflammatory abilities against novel coronavirus SARS-CoV-2 via suppression of NF-κB signaling pathway. *Pharm. Res.* **158**, 104850. https://doi.org/10.1016/j.phrs.2020.104850 (2020).
42. Rhim, J. S. *et al.* Biological characteristics and viral susceptibility of an African green monkey kidney cell line (Vero). *Proc. Soc. Exp. Biol. Med.* **132**, 670–678. https://doi.org/10.3181/00379727-132-34285 (1969).
43. Runfeng, L. *et al.* Lianhuaqingwen exerts anti-viral and anti-inflammatory activity against novel coronavirus (SARS-CoV-2). *Pharm. Res.* **156**, 104761. https://doi.org/10.1016/j.phrs.2020.104761 (2020).
44. Raval, B. P., Suthar, M. P. & Patel, R. K. Potent in vitro anti-tumor activity of Symplocos racemosa against leukemia and cervical cancer. *Electron J. Biol.* **5**, 89–91 (2009).
45. Subedi, R. K., Kang, K. W. & Choi, H.-K. Preparation and characterization of solid lipid nanoparticles loaded with doxorubicin. *Eur. J. Pharm. Sci.* **37**, 508–513. https://doi.org/10.1016/j.ejps.2009.04.008 (2009).
46. Kim, M.-H. *et al.* Formulation and evaluation of nanostructured lipid carriers (NLCs) of 20 (S)-protopanaxadiol (PPD) by Box-Behnken design. *Int. J. Nanomed.* **14**, 8509. https://doi.org/10.2147/IJN.S215835 (2019).
47. Xu, Q. *et al.* Soybean-based surfactants and their applications. *Soybean Appl. technol.* https://doi.org/10.5772/15261 (2011).
48. Freitas, C. & Müller, R. H. Effect of light and temperature on zeta potential and physical stability in solid lipid nanoparticle (SLN™) dispersions. *Int. J. Pharm.* **168**, 221–229. https://doi.org/10.1016/S0378-5173(98)00092-1 (1998).
49. Teeranachaideekul, V. *et al.* Cetyl palmitate-based NLC for topical delivery of Coenzyme Q10–Development, physicochemical characterization and in vitro release studies. *Eur. J. Pharm. Biopharm.* **67**, 141–148. https://doi.org/10.1016/j.bfopcu.2015.10.001 (2007).
50. Jeon, W.-J. *et al.* Antiviral lipid nanocarrier loaded with remdesivir effective against SARS-CoV-2 in vitro model. *Int. J. Nanomed.* https://doi.org/10.2147/IJN.S391462 (2023).
51. Sahakijpijarn, S. *et al.* Development of remdesivir as a dry powder for inhalation by thin film freezing. *Pharmaceutics* **12**, 1002. https://doi.org/10.3390/pharmaceutics12111002 (2020).

52. Pardeike, J. *et al.* Development of an itraconazole-loaded nanostructured lipid carrier (NLC) formulation for pulmonary application. *Int. J. Pharm.* **419**, 329–338. https://doi.org/10.1016/j.ijpharm.2011.07.040 (2011).
53. Bunjes, H., Westesen, K. & Koch, M. H. Crystallization tendency and polymorphic transitions in triglyceride nanoparticles. *Int. J. Pharm.* **129**, 159–173. https://doi.org/10.1016/0378-5173(95)04286-5 (1996).
54. Zhang, X. *et al.* Preparation of a dispersible PEGylate nanostructured lipid carriers (NLC) loaded with 10-hydroxycamptothecin by spray-drying. *Chem. Pharm. Bull.* **56**, 1645–1650. https://doi.org/10.1248/cpb.56.1645 (2008).
55. Luan, J. *et al.* Design and characterization of Amoitone B-loaded nanostructured lipid carriers for controlled drug release. *Drug Deliv.* **20**, 324–330 (2013).
56. Wissing, S., Kayser, O. & Müller, R. Solid lipid nanoparticles for parenteral drug delivery. *Adv. Drug deliv. Rev.* **56**, 1257–1272. https://doi.org/10.1016/j.addr.2003.12.002 (2004).
57. Yang, X. *et al.* Preparation and characterization of 4-dedimethylamino sancycline (CMT-3) loaded nanostructured lipid carrier (CMT-3/NLC) formulations. *Int. J. Pharm.* **450**, 225–234. https://doi.org/10.1016/j.ijpharm.2013.04.021 (2013).
58. Zhigaltsev, I. V. *et al.* Development of a weak-base docetaxel derivative that can be loaded into lipid nanoparticles. *J. Controll. Release* **144**, 332–340. https://doi.org/10.1016/j.jconrel.2010.02.029 (2010).
59. Neupane, Y. R. *et al.* Lipid based nanocarrier system for the potential oral delivery of decitabine: Formulation design, characterization, ex vivo, and in vivo assessment. *Int. J. Pharm.* **477**, 601–612. https://doi.org/10.1016/j.ijpharm.2014.11.001 (2014).
60. Nimbkar, S. *et al.* Medium chain triglycerides (MCT): State-of-the-art on chemistry, synthesis, health benefits and applications in food industry. *Comp. Rev. Food Sci. Food Safe.* **21**, 843–867. https://doi.org/10.1111/1541-4337.12926 (2022).
61. Wang, S.-W. *et al.* GPR84 regulates pulmonary inflammation by modulating neutrophil functions. *Acta Pharmacol. Sin.* https://doi.org/10.1038/s41401-023-01080-z (2023).
62. Diehl, N. & Schaal, H. Make yourself at home: Viral hijacking of the PI3K/Akt signaling pathway. *Viruses* **5**, 3192–3212. https://doi.org/10.3390/v5123192 (2013).
63. Saito, R.d.F., *et al.* Phosphatidylcholine-derived lipid mediators: The crosstalk between cancer cells and immune cells. *Front. Immunol.* **13**, 768606. https://doi.org/10.3389/fimmu.2022.768606 (2022).
64. Wanten, G. J. & Naber, A. H. Cellular and physiological effects of medium-chain triglycerides. *Mini Rev. Med. Chem.* **4**, 847–857. https://doi.org/10.2174/1389557043403503 (2004).
65. Place, T. L., Domann, F. E. & Case, A. J. Limitations of oxygen delivery to cells in culture: An underappreciated problem in basic and translational research. *Free Radic. Biol. Med.* **113**, 311–322. https://doi.org/10.1016/j.freeradbiomed.2017.10.003 (2017).
66. Capes-Davis, A. & Ian Freshney, R. *Freshney's Culture of Animal Cells: A Manual of Basic Technique and Specialized Applications* (Wiley, 2021).
67. Wu, B. *et al.* Acute kidney injury associated with remdesivir: A comprehensive pharmacovigilance analysis of COVID-19 reports in FAERS. *Front. Pharma.* **13**, 692828. https://doi.org/10.3389/fphar.2022.692828 (2022).
68. van Laar, S. A. *et al.* Liver and kidney function in patients with Covid-19 treated with remdesivir. *Br. J. Clin. Pharmacol.* **87**, 4450–4454. https://doi.org/10.1111/bcp.14831 (2021).
69. Milkova, V. *et al.* Remdesivir-loaded nanoliposomes stabilized by chitosan/hyaluronic acid film with a potential application in the treatment of coronavirus infection. *Neurol. Int.* **15**, 1320–1338. https://doi.org/10.3390/neurolint15040083 (2023).
70. Viegas, C. *et al.* Solid lipid nanoparticles vs. nanostructured lipid carriers: A comparative review. *Pharmaceutics* **15**, 1593. https://doi.org/10.3390/pharmaceutics15061593 (2023).

Acknowledgements

Financial support provided by the Research Council of the University of Tehran is gratefully appreciated.

Author contributions

H.G. and F.A. contributed to the conception and design of the work. Material preparation, data collection, and analysis were performed by F.A. and S.Z.C. The first draft of the manuscript was written by F.A. H.G. and S.Z.C. reviewed and revised the initial draft. Also, H.G. and S.Z.C. contributed to data interpretation. Artworks are prepared by S.Z.C. and F.A. All authors read and approved the final manuscript.

Competing interests

The authors declare no competing interests.

Additional information

Correspondence and requests for materials should be addressed to H.G.